Atomistic Deformation Modes in Strong Covalent Solids

Yi Zhang,[1] Hong Sun,[1,2,*] and Changfeng Chen[2,*]

[1]*Department of Physics, Shanghai Jiao Tong University, Shanghai 200030, China*

[2]*Department of Physics and High Pressure Science and Engineering Center, University of Nevada, Las Vegas, Nevada 89154, USA*

(Received 9 December 2004; published 15 April 2005)

We report on a first-principles study of the structural deformation modes in diamond, cubic boron nitride (*c*-BN), and cubic BC_2N. We show that (i) the diamond C-C bonds remain strong up to the breaking point, leading to the large and nearly identical shear and tensile strength, (ii) *c*-BN exhibits a shear failure mode different from that in diamond and a significant softening in the B-N bonds at large tensile strains long before the bond breaking, and (iii) cubic BC_2N displays a large disparity between the shear and tensile strength, contrary to the expectation for the hybrid of diamond and *c*-BN. We examine the microscopic bond-breaking processes to elucidate the atomistic mechanisms for the deformation modes and the implications for material strength.

DOI: 10.1103/PhysRevLett.94.145505 PACS numbers: 62.20.Fe, 81.40.Jj

Diamond is the hardest material known and cubic boron nitride (*c*-BN) is second only to diamond in hardness with significantly improved thermal stability. In recent years, considerable efforts have been devoted to the synthesis [1–5] and modeling [6–10] of ternary BCN materials with the expectation that a hybrid of the top two superhard materials may lead to the benefit of the best of the two worlds, namely, an enhanced hardness (over that of *c*-BN) and an improved thermal stability (over that of diamond). Two recent experiments reported [4,5] successful synthesis of cubic BC_2N that indeed shows excellent thermal stability superior to that of diamond and a hardness exceeding that of *c*-BN. To understand the microscopic structural behavior of these strong covalent solids, first-principles studies on their deformation and failure modes are highly desirable. While the equilibrium properties such as the bulk and shear moduli are routinely used as indicators for material hardness, a more stringent test is provided by the ideal strength, i.e., the stress at which a perfect crystal becomes unstable [11,12], that sets an upper bound for material strength. This is because material deformation is strain dependent and simple extrapolations from the results near the equilibrium may not be reliable. More importantly, studies of the stress-strain relations and the underlying atomistic bond-breaking processes can provide important insights into the fundamental aspects of the deformation and failure modes critical to the understanding of the mechanical behavior. However, of these top superhard materials, only diamond has been previously studied for structural instabilities under large strains [13–15]. The microscopic mechanisms for and differences in their structural deformation and failure modes remain largely unexplored.

In the present work we aim to further examine the microscopic bond-breaking process in diamond and to establish an atomistic description for the structural deformation modes in *c*-BN and cubic BC_2N. We find that the B-N bonds in *c*-BN soften under large tensile strains long before its bond breaking, in contrast to the situation in diamond where the C-C bonds remain strong up to the breaking point. *c*-BN also shows a shear deformation mode different from that in diamond. Meanwhile, cubic BC_2N exhibits a much larger disparity between its ideal shear and tensile strength. It is caused by a deformation mode involving a sequence of individual bond-breaking events, which is different from those in diamond and *c*-BN where all the relevant bonds break simultaneously. On the other hand, in contrast to the rich varieties of the tensile failure modes, the shear modes in all three materials follow a common pattern of remaining strong up to the bond-breaking point and undergo a large volume expansion to the graphitic phase with simultaneous breaking of all the relevant bonds.

The total-energy calculations were carried out using the local-density-approximation (LDA) pseudopotential scheme with a plane-wave basis set [16–18]. The norm-conserving Troullier-Martins pseudopotentials [19] were used with cutoff radii of 1.3, 1.3, 1.5 a.u. for N, C, and B, respectively. The exchange-correlation functional of Ceperley and Alder [17] as parametrized by Perdew and Zunger [20] was used. The total energy of the structures was minimized by relaxing the structural parameters using a quasi-Newton method [21]. The total-energy and stress calculations used an eight-atom zinc-blende-structured unit cell, an $8 \times 8 \times 8$ Monkhorst-Pack [22] *k*-point grid, and an 80 Ry energy cutoff. The error in the calculated stresses due to the energy cutoff and *k*-point grid was less than 0.1 GPa based on convergence tests. The quasistatic ideal strength and relaxed loading path in the various directions was determined using a method described previously [23,24]. The lattice vectors were incrementally deformed in the direction of the applied strain. At each step the atomic basis vectors and all the atoms inside the unit cell were simultaneously relaxed until all residual components of the Hellmann-Feynman stress tensor orthogonal to the applied strain are less than 0.1 GPa. The

shape of the unit cell is determined by the full atomic relaxation without any imposed boundary conditions. For all the materials considered, tensile stresses along various crystallographic directions were calculated and the weakest direction in each case was identified; the shear stresses in the easy slip planes were also identified and the critical shear stress obtained. We also carried out dynamic phonon calculations using the ABINIT code [25] to examine the stability of the strained structures [26–28].

Figure 1 shows the calculated stress-strain relation and the snapshots of the strained structures right before and after the bond-breaking points for diamond. We have identified the body-diagonal $\langle 111 \rangle$ direction as the weakest tensile direction, in agreement with the previous result [15]. With the x ($[11\bar{2}]$) and z ($[111]$) axis indicated in the figure, the positive shear stress σ is given by $\sigma_{13} = \sigma_{31} > 0$ and the other seven components of the stress tensor being null. The ideal shear strength is obtained under the (111) $\langle 11\bar{2} \rangle$ shear. The calculated tensile and shear ideal strength for diamond are 92.9 GPa and 96.3 GPa, respectively. These values are in excellent agreement with previous results [13–15]. They lead to a shear-to-tensile strength ratio of 1.0366, or a disparity of 3.66% between them. We now examine the bond-breaking process in diamond. The C-C bonds remain very strong up to the bond-breaking points under tensile or shear strains. At the critical *tensile* strain ($\epsilon = 0.15$), the stress has only decreased slightly from the peak value. The corresponding structural snapshot shows significant buckling in the (111) planes, indicating a strong sp^3 bonding character. The structural failure occurs at $\epsilon = 0.16$, where the interlayer bonds in the $\langle 111 \rangle$ direction break up [29] and the layers in the (111) planes become essentially flat, signaling a dominant sp^2 bonding character. The negative stress ($\sigma_{33} < 0$ in Fig. 1) shows an expansion tendency of the structure in the z direction after the bond breaking at $\epsilon = 0.16$. The corresponding bond length of 2.292 Å (see Table I) is much larger than the breaking bond length of 2.07 Å at the saddle point in a diamond-to-graphite transformation [30]. The C-C bonds in diamond also remain strong up to the breaking point at the critical *shear* strain of $\epsilon = 0.350$ where the sp^3 bonding character is clearly seen. Above the critical shear strain, a transformation into the graphite structure occurs with a 53% volume expansion. It is noticed that all the C-C bonds in diamond responsible for the structural failure break simultaneously under tensile or shear strains.

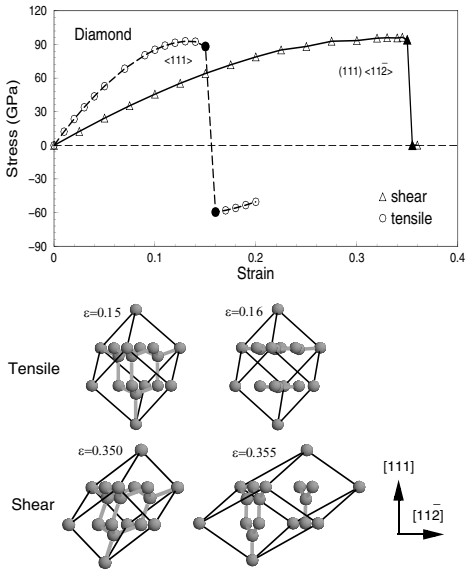

FIG. 1. The stress-strain relations for the shear and tensile deformation in diamond. Also shown are the "snapshots" of the strained structures right before and after the bond-breaking points, corresponding to the filled symbols in the stress-strain plot.

c-BN has a calculated (see Fig. 2) tensile and shear ideal strength of 65.6 GPa and 70.5 GPa, respectively, yielding a 7.47% disparity between them. These values are obtained under the $\langle 111 \rangle$ tensile and (111) $\langle 11\bar{2} \rangle$ shear as in diamond. Despite their similarities, c-BN exhibits significant differences in its structural deformation modes. First, unlike the C-C bonds in diamond that remain strong up to the breaking point, the B-N bonds soften considerably under the *tensile* strain long before the bond breaking. The peak tensile stress occurs at the strain $\epsilon = 0.11$ but the interlayer sp^3 bonding persists up to $\epsilon = 0.14$ where significant buckling still exists and the B-N bond length of 1.967 Å is just below the value at the transformation into the graphitic BN phase [31]. All of these point to a strained cubic structure up to $\epsilon = 0.14$. Above this critical tensile strain, the transition to the graphitic phase occurs with a significantly increased bond length of 2.213 Å (see Table I). However, the breakdown of the elasticity occurs at $\epsilon = 0.11$, followed by a gradual reduction of the tensile stress. This is in contrast to the sharp drop in the tensile stress near the critical strain in diamond. This bond softening under

TABLE I. Calculated bond lengths in diamond, c-BN, and BC_2N right before and after their breaking points under tensile or shear strains.

Diamond	tensile strain	0.15	0.16	
	C-C bond (Å)	1.850	2.292	
	shear strain	0.350	0.355	
	C-C bond (Å)	1.715	3.423	
c-BN	tensile strain	0.14	0.15	
	B-N bond (Å)	1.967	2.213	
	shear strain	0.370	0.375	
	B-N bond (Å)	1.705	3.325	
BC_2N	tensile strain	0.09	0.10	0.12
	C-N bond (Å)	1.868	2.025	2.335
	B-N bond (Å)	1.767	1.814	2.186
	shear strain	0.270	0.275	
	B-C bond (Å)	1.690	3.251	
	C-C bond (Å)	1.621	3.254	
	C-N bond (Å)	1.664	3.257	
	B-N bond (Å)	1.754	3.263	

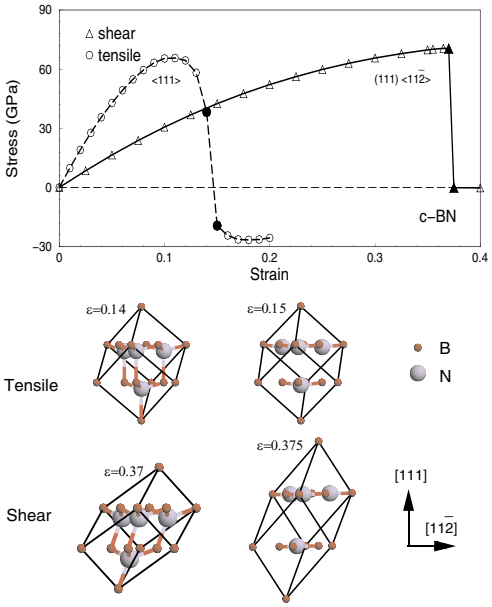

FIG. 2 (color online). The stress-strain relations and the snapshots (corresponding to the filled symbols in the top figure) of the strained structures right before and after the bond-breaking points for *c*-BN.

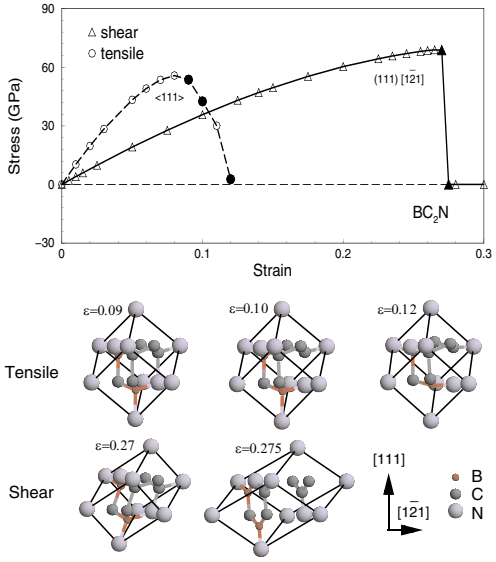

FIG. 3 (color online). The stress-strain relations and the snapshots (corresponding to the filled symbols in the top figure) of the strained structures right before and after the bond-breaking points for cubic BC_2N.

large tensile strains is the result of the charge depletion on the partially ionic B-N bonds; it reduces the ideal tensile strength of *c*-BN compared to its shear strength, yielding the increased disparity between them. Second, although *c*-BN also undergoes a cubic-to-graphitic transformation with a 49% volume expansion under the same (111) $\langle 11\bar{2}\rangle$ *shear* strain as in diamond, its shear deformation mode leads to a structure with the graphitic layers in the (111) planes after the transformation. This is in contrast to the case of diamond where the graphitic layers are in the (11$\bar{2}$) planes. This difference is also caused by the partially ionic nature of the B-N bonds in *c*-BN. Further details of the shear deformation in *c*-BN will be presented elsewhere. Here we notice that all the B-N bonds responsible for the structural failure also break simultaneously under tensile or shear strains.

Among many possible bonding configurations in cubic BC_2N, we identified an optimal structure that completely avoids the energetically unfavorable N-N and B-B bonds and has the remaining four types of bonds evenly distributed in all the body-diagonal directions [10,32]. This optimal cubic BC_2N has a shear (tensile) ideal strength of 68.8 GPa (55.8 GPa). Given its close structural and bonding characters to diamond and *c*-BN, the 23.3% disparity between the shear and tensile strength is surprisingly large. A close examination of the atomistic deformation modes reveals its microscopic mechanism. Figure 3 shows that the relevant bonds in cubic BC_2N break simultaneously under the *shear* strain [33], yielding a large critical shear stress. However, it goes through a sequence of individual bond-breaking events under a *tensile* strain. The latter process leads to an early breakdown of elasticity at $\epsilon = 0.08$ and a significantly reduced tensile strength. Substantial interlayer bonding and buckling are clearly visible even after two bonds break (C-N at $\epsilon = 0.10$ and B-N at $\epsilon = 0.12$) under the tensile strain. An examination of the charge density on the various bonds at equilibrium and under large tensile strains provides an especially revealing picture for the atomistic tensile deformation mode. Figure 4 shows that the C-N bond [in the ($\bar{1}$01) plane] has its charge significantly reduced from the equilibrium value at the tensile strain $\epsilon = 0.1$ and breaks first (see the bond length in Table I). It weakens the zigzag -N-B-N-C- chain in the [111] direction. Consequently, the B-N bonds in this chain stretch and break at $\epsilon = 0.12$ (see Table I), accompanied by a sharp decline of charge on the bond. Meanwhile, the C-C [in the (0$\bar{1}$1) plane] and the C-B [in the (1$\bar{1}$0) plane]

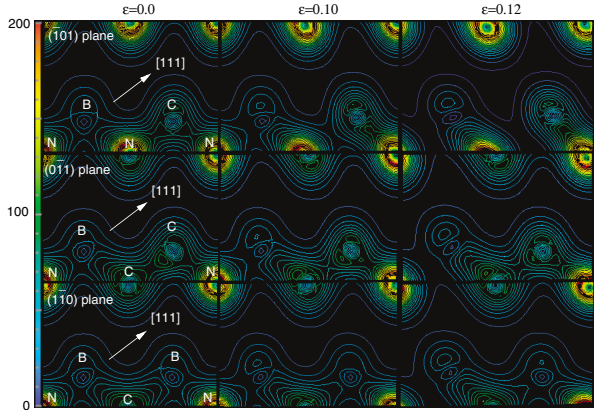

FIG. 4 (color). The charge density (in electrons/cell) for cubic BC_2N in the ($\bar{1}$01), (0$\bar{1}$1), and (1$\bar{1}$0) planes at the equilibrium ($\epsilon = 0$) and bond-breaking points ($\epsilon = 0.10, 0.12$).

bonds remain intact at $\epsilon = 0.12$ as evidenced by the large amount of charge still on the bonds. The corresponding bond lengths of 1.660 Å (C-C) and 1.748 Å (C-B) are well below their breaking bond lengths [29]. The resultant large disparity between its shear and tensile strength reveals the structural vulnerability of cubic BC_2N to fractures of tensile type (e.g., cleavage) despite its high microhardness that is closely correlated with the shear strength [34]. It is interesting to note that the sequential bond breaking of BC_2N under the tensile loading induces some lateral atomic movements, resulting in a small shear strain (<0.015) before cleavage.

We have performed dynamic phonon calculations for diamond, *c*-BN, and cubic BC_2N and found no phonon instabilities up to the bond-breaking points in all the cases. This lack of (acoustic and optical) phonon softening affirms the stability of the strained structures studied here.

Finally, we summarize the main results of the present work. (i) The C-C bonds in diamond remain strong up to the breaking point under tensile or shear strains, leading to the large and close tensile and shear strength. (ii) The B-N bonds in *c*-BN soften long before the breaking point under large tensile strains but remain strong up to the breaking point under shear strains. As a result, *c*-BN exhibits a larger disparity between its tensile and shear strength compared to diamond. *c*-BN is also different from diamond in its shear deformation modes leading to the graphitic phase. (iii) Cubic BC_2N has an unexpectedly large disparity between its shear and tensile strength. It is caused by a *tensile* deformation mode that involves a sequence of individual bond-breaking events that significantly reduce the tensile strength. Meanwhile, there is no bond softening or sequential bond breaking under *shear* strains in all three materials. These results demonstrate that while mixing two (or more) materials can lead to great benefits such as the improved thermal stability in BC_2N over that of diamond, the resulted richer bonding options could introduce weak links, such as the zigzag chain containing the C-N bonds in BC_2N, that reduce the strength to below that for either of the parent materials.

This work was supported by the DOE under Cooperative Agreement DE-FC52-01NV14049 at UNLV. H. S. was also supported by the NNSF of China under Grant No. 10274050 and the High Performance Computing Center at Shanghai Jiao Tong University.

*Correspondence should be addressed to these authors.

[1] S. Nakano *et al.*, Chem. Mater. **6**, 2246 (1994).
[2] E. Knittle *et al.*, Phys. Rev. B **51**, 12149 (1995).
[3] T. Komatsu *et al.*, J. Mater. Chem. **6**, 1799 (1996).
[4] V. L. Solozhenko *et al.*, Appl. Phys. Lett. **78**, 1385 (2001).
[5] Y. Zhao *et al.*, J. Mater. Res. **17**, 3139 (2002).
[6] W. R. L. Lambrecht and B. Segall, Phys. Rev. B **40**, 9909 (1989).
[7] Y. Tateyama *et al.*, Phys. Rev. B **55**, R10161 (1997).
[8] J. C. Zheng *et al.*, J. Phys. Condens. Matter **11**, 927 (1999).
[9] R. Q. Zheng *et al.*, Appl. Phys. Lett. **75**, 2259 (1999).
[10] H. Sun *et al.*, Phys. Rev. B **64**, 094108 (2001).
[11] A. Kelly and N. H. Macmillan, *Strong Solids* (Clarendon, Oxford, 1986), 3rd ed., pp. 1–56.
[12] J. W. Morris, Jr. *et al.*, in *Phase Transformations and Evolution in Materials*, edited by P. E. Turchi and A. Gonis (TMS, Warrendale, PA, 2000), pp. 187–207.
[13] D. Roundy and M. L. Cohen, Phys. Rev. B **64**, 212103 (2001).
[14] H. Chacham and L. Kleinman, Phys. Rev. Lett. **85**, 4904 (2000).
[15] R. H. Telling *et al.*, Phys. Rev. Lett. **84**, 5160 (2000).
[16] J. Ihm, A. Zunger, and M. L. Cohen, J. Phys. C **12**, 4409 (1979).
[17] D. M. Ceperley and B. J. Alder, Phys. Rev. Lett. **45**, 566 (1980).
[18] M. L. Cohen, Phys. Scr. **T1**, 5 (1982).
[19] N. Troullier and J. L. Martins, Phys. Rev. B **43**, 1993 (1991).
[20] J. P. Perdew and A. Zunger, Phys. Rev. B **23**, 5048 (1981).
[21] B. G. Pfrommer *et al.*, J. Comput. Phys. **131**, 233 (1997).
[22] H. J. Monkhorst and J. D. Pack, Phys. Rev. B **13**, 5188 (1976).
[23] D. Roundy *et al.*, Philos. Mag. A **81**, 1725 (2001).
[24] D. Roundy *et al.*, Phys. Rev. Lett. **82**, 2713 (1999).
[25] X. Gonze, Phys. Rev. B **55**, 10337 (1997); X. Gonze and C. Lee, *ibid.* **55**, 10355 (1997).
[26] S. H. Jhi *et al.*, Phys. Rev. Lett. **87**, 075503 (2001).
[27] J. Li and S. Yip, Comput. Model. Eng. Sci. **3**, 219 (2002).
[28] D. M. Clatterbuck *et al.*, Phys. Rev. Lett. **91**, 135501 (2003).
[29] In plotting the structural snapshots, we used the RASMOL code (see http://www.umass.edu/microbio/rasmol/). The criteria for bond breaking are obtained by increasing the bond lengths continuously in a series of testing plots. The values are 1.964 Å, 2.003 Å, 2.075 Å, and 2.116 Å for the C-N, C-C, B-N, and B-C bond, respectively.
[30] S. Fahy *et al.*, Phys. Rev. B **34**, 1191 (1986).
[31] R. M. Wentzcovitch *et al.*, Phys. Rev. B **38**, 6191 (1988).
[32] Y. Zhang, H. Sun, and C. F. Chen, Phys. Rev. Lett. **93**, 195504 (2004).
[33] We examined all six shear directions in the easy slip (111) plane of cubic BC_2N and determined the weakest critical stress under the (111) $[1\bar{2}1]$ shear.
[34] D. M. Teter, Mater. Res. Bull. **23**, 22 (1998).